

Compound-tunable embedding potential method and its application to calcium niobate crystal CaNb_2O_6 with point defects containing tantalum and uranium

D. A. Maltsev ^{1,*}, Yu. V. Lomachuk ¹, V. M. Shakhova ^{1,2}, N. S. Mosyagin ¹, L. V. Skripnikov ^{1,2} and A. V. Titov ^{1,†}

¹*B.P. Konstantinov Petersburg Nuclear Physics Institute of National Research Center “Kurchatov Institute”*

(NRC “Kurchatov Institute” - PNPI), Gatchina, Leningrad district 188300, Russia

²*Saint Petersburg State University, 7/9 Universitetskaya nab., 199034 St. Petersburg, Russia*



(Received 24 November 2020; accepted 5 April 2021; published 4 May 2021)

The compound-tunable embedding potential (CTEP) method developed for simulating the influence of environment on a fragment in the ionic-covalent crystal is presented in the form of a linear combination of particular short-range semilocal pseudopotentials for the atoms of nearest environment and the long-range Coulomb potentials from optimized fractional point charges centered on both nearest and more distant atoms of the environment. A pilot application of the CTEP method to calcium niobate crystal, CaNb_2O_6 , is performed. A very good agreement of the electronic density and interatomic distances within the relaxed fragment with those of the original periodic crystal calculation is attained. Calcium niobate crystal can be considered as an idealized fersmite ($\text{CaNb}_{2-x}\text{Ta}_x\text{O}_6$, $x \approx 0.3$) mineral when neglecting the contributions of the impurities with smaller molar fractions, and substitution $\text{Nb} \rightarrow \text{Ta}$ is considered here as a point Ta defect in CaNb_2O_6 . Besides, uranium-containing point defects are also studied since the euxenite group minerals, to which fersmite belongs, are considered as prospective matrices for long-term immobilization of high-level waste. The chemical shifts of $K_{\alpha_{1,2}}$ and $K_{\beta_{1,2}}$ lines of x-ray emission (fluorescence) spectra in niobium are evaluated to analyze its chemical state in the crystal. Potential of CTEP for studying properties of point defects containing f and heavy d elements with relativistic effects, extended basis set, and broken crystal symmetry taken into account is discussed.

DOI: [10.1103/PhysRevB.103.205105](https://doi.org/10.1103/PhysRevB.103.205105)

I. INTRODUCTION

Impressive recent achievements in creating experimental facilities to study local atomic-scale electronic structures in material science like x-ray free-electron lasers, synchrotrons [1], high harmonic generation sources [2], etc. open a new era in investigating materials and defects containing heavy transition metals (d elements), lanthanides and actinides (f elements); we will designate all these atoms as d/f elements below. However, capabilities of direct theoretical electronic structure modeling of such materials on the atomic scale are yet limited. There were developed quantum-chemical packages, in particular, VASP [3] and CASTEP [4], for plane-wave studies of periodic systems which allow one to treat d/f elements using ultrasoft [5], projected augmented wave (PAW) [6], and norm-conserving core pseudopotentials (PPs or effective core potentials) [7,8], which were further developed in a series of papers (see Refs. [9–11] and references therein); their relative efficiency is compared, e.g., in Ref. [12]. Using these PPs one can seriously reduce the computational cost when balancing the way and radii of smoothing the valence orbitals in atomic cores with the energy cutoff value for plane waves to attain desirable final accuracy. Nevertheless, only a *moderate* number of electrons per atom can be explicitly used in mainstream calculations of solids including

d/f elements. Such PPs, in which only a part of the shells localized in the outer-core region is treated explicitly (e.g., $4f$ in lanthanides and $5f$ in actinides), whereas the other ones (correspondingly, $[...]4spd$ in lanthanides and $[...]5spd$ in actinides) as described within the PPs are known as “semi-core” pseudopotentials (call them below the “medium-core” PPs or mc-PPs for brevity to distinguish them from the small-core PPs or sc-PPs), since the average radii of the atomic orbitals with the same principal quantum number are rather close (particularly for those localized in the core region). They are limited by accuracy as one can see, e.g., from analysis of large-core PPs (only valence electrons are treated explicitly), small-core PPs [valence and all the outer-core shells with the same principal quantum number(s) are treated explicitly], and medium-core ones for uranium and silver in Ref. [13]. The medium-core PPs for uranium, in which 78 ($[...]5spd$) or 68 ($[...]5sp$) electrons are in core, can be not sufficient in applications because of closeness of levels with different occupation numbers of the $6d$ and/or $5f$ shells having one-electron energies close to those for the valence $7s$ and/or $7p$ shells.

There are two standard options available for lanthanides and actinides, e.g., in framework of the VASP package with popular PAW potentials [14], for which the $4f$ and $5f$ orbitals, correspondingly, can be treated (1) as valence states or (2) as f electrons in the core (with the precaution that “these potentials are not expected to work reliably”). It was recently demonstrated in DFT calculations of xenotime crystal, YPO_4 [15] with the uranium atom as a point defect [the substitution

*malcev_da@pnpi.nrcki.ru

†titov_av@pnpi.nrcki.ru

Y(III) \rightarrow U(III,IV) is considered], that its $5f^{n_c+n_b}$ electrons both occupy *localized* states (“ $5f$ -in-core” or $5f^{n_c}$) and give notable contribution to the bonding of U with neighboring oxygen atoms (“ $5f$ -in-bond” or $5f^{n_b}$). The $5f^{n_c}$ designation means that $n_c = 3$ for U(III) and $n_c = 2$ for U(IV), whereas $5f^{n_b}$ means that the atomic $5f$ orbitals are shares of the valence crystal orbitals within the CO LCAO approximation, such that $n_b \approx 0.3$ and $n_b \approx 0.7$ for the U(III) and U(IV) point defects in xenotime, correspondingly. Note that the use of localized basis sets in CO LCAO studies of periodic systems is computationally preferable compared to the plane-wave investigations in many applications (e.g., see discussion in Ref. [16]) when small-core PPs should be used to attain good accuracy.

Unfortunately, improvement of computational accuracy for electronic properties of materials containing heavy transition elements, lanthanides and actinides and, in particular, for those concentrated in atomic cores of d/f elements, i.e., properties of atoms-in-compounds (AiC) [17–22] are yet hampered by several challenges in quantum chemical description of such systems. They first include necessity of highest-level treatment of relativistic and correlation effects simultaneously, including those for outer-core shells (see last reviews on PPs for lanthanides [23] and actinides [24]). Besides, polyvalent d/f element compounds often have pronounced multireference character of their electronic structure and a high density of low-lying electronic states, whose mixing can take place in practical calculations. As a result, opportunities for direct *ab initio* study of materials containing d/f elements with required accuracy can be blocked by unacceptable computational cost. An alternative way to explore such a material is to reduce their studying to a molecular-type investigation of some of its fragments, which are of particular interest, assuming that relaxation of the rest of the crystal (environments of the fragments) in processes under consideration is negligible. In this case, one can consider influence of the environment on a fragment by some approximate *embedding potential* to improve the quality of description of phenomena localized on the fragment using extended possibilities of molecular methods which include sophisticated treatment of relativistic and correlation effects. Such a fragment with embedding potential is usually called the “embedded cluster” or “cluster, embedded in a crystal.”

The embedding potential theories (see Refs. [25,26] and references therein) are based on the idea of freezing the external environment of a chosen crystalline fragment (cluster of atoms); they are conceptually similar to the core pseudopotential theories (e.g., see Refs. [12,13]) which are originated by the frozen core approximation in atoms. The embedding theories, which provide high accuracy of simulating the interaction of a fragment with environment, are of particular interest for studying point defects, localized properties, and processes in solids and other polyatomic systems, first of all if they contain d/f elements.

Among the phenomena of increasing interest, one could highlight opening new possibilities to study magnetic structure of materials characterized by specific electronic configuration of d/f elements (see Refs. [27,28] and references therein), localized excitations in crystals and matrices (molecular rotors [29], chimeras and intrinsic localized modes

(discrete breathers) [30], electronic transitions and magneto-optical effects in point defects [31] including laser generation processing [32,33]), new physics in ferroelectrics (see Refs. [34–37] and references therein), etc.

Direct *ab initio* study of electronic structure of polyatomic and periodic systems containing d/f elements with high accuracy is problematic to date. Excitation energies for valence electrons in them can be very small, within errors of density functional theory (DFT) approximation. The situation is most difficult for light actinides, which show both lanthanidelike and transition-metal-like behavior. Therefore, calibration of the exchange-correlation DFT functionals should be done to choose its appropriate version, which provides the correct valence state of d/f elements in a compound under consideration. In turn, calculation of an ionic-covalent crystal fragment of small size (including a central d/f element and its first anionic coordination sphere) using the embedding potentials and combining [36,38] advanced two-component (relativistic) versions of density functional [39] and coupled-cluster (see Refs. [40–44] and references therein) theories can be done in practice now. Furthermore, one can perform a relativistic calculation of a larger cluster with actinide impurities and vacancies to take relaxation of its neighbors into account using a chosen (calibrated) DFT functional. In total, the relativistic coupled-cluster (RCC) corrections to the DFT calculation of the small-size clusters can be efficiently applied—a pilot combined study of such a kind was performed for PbTiO_3 crystal [36] to search for a new physics (Schiff moment of the ^{207}Pb nucleus). In the cases when one needs to consider some minimal-size cluster that cannot be well studied within the coupled-cluster techniques, a combination of the DFT with the methods developed for the strong correlation problem and discussed in the following two paragraphs can be applied. In the DFT study of the embedded cluster of a “moderate size” one can use accurate sc-PP versions and large enough atomic basis sets in contrast to the periodic DFT studies.

Theories of embedding the clusters in crystals [25,26] are actively used in solid-state studies. We mention here only a few recent developments of the embedding theories. In a series of papers (see Ref. [45] and references in Ref. [46]), density matrix embedding theory, DMET, is developed where single-particle density matrix is the quantum variable rather than the Greens function used in the parent dynamic mean-field theory, DMFT (see Refs. [47,48] and references therein), for a strong correlation problem. It describes a finite-size fragment in the environment such that the local density of states can be obtained when working with a limited (“compact”) Fock space of environmental states (“bath”) when using the Schmidt decomposition for the wave function of the whole system (singular value decomposition theorem, e.g., see Ref. [49]). The idea of DMET is to define an approximate bath space and embed an impurity in this bath space. It was found that DMET yields very accurate ground-state energies for the Hubbard model [50,51] and geometries around equilibrium for some quantum chemical systems [46,52], though a precaution is required in evaluating bond dissociation [53], etc. A key problem in DMET is to find optimal bath states, and several ways are developed here [46]. To our knowledge, however, all DMET studies of compounds of d/f elements

are performed within the Hubbard model and not quantum chemical consideration, which is the subject of our paper.

Note that the quantum embedding methods based on the dynamic mean-field theory directly have also made good progress in different ways. We mention here only some of them. Applications of the DMFT-like correlated fluctuations' technique for environment to a ground-state wave-function embedding approach is considered in Ref. [54] in the example of one-dimensional Hubbard chain. This approach provides an opportunity for a systematically improvable, short-time wave function analog to DMFT. The embedding problem in molecular systems is discussed in Ref. [55] for the hemocyanin protein, in which the stabilization of the experimentally observed di-Cu singlet for the butterfly Cu₂O₂ core is, in particular, explained. In Ref. [56], a maximally localized dynamically embedding is considered to resolve the Anderson impurity model based on an extended exact diagonalization method. The authors report that quantum impurity models with as few as three bath sites can reproduce both the Mott transition and the Kondo physics, thus opening a more accessible route to the description of time-dependent phenomena. Embedding theory applications to a diluted solid is considered in Ref. [57], where the phase diagram of superlattice structures of f elements on substrates is investigated, assessing the required conditions to obtain the diluted Kondo superlattices. Application of DMFT to periodic systems containing f elements— γ cerium, cerium sesquioxide (Ce₂O₃), and samarium telluride (SmTe)—is considered, in particular, in Ref. [58] in combination with DFT using CASTEP code.

Going beyond the self-consistent field approximation for environment, Höfener and colleagues considered DFT-based methods which encompass (1) wave-function theory-in-DFT (WFT-in-DFT) formulations of the response theory, which allow one to consider electronic excitations, etc. mainly localized in a fragment, and (2) DFT-based consideration of a fragment in a compound (DFT-in-DFT), when any selected functional can fail to provide a quantitatively correct description of all the subsystems in the compound of interest, see Refs. [59–62] and references therein. These approaches allow one to take account of the environmental relaxation due to perturbation by a point defect, etc. in a small fragment. To attain a required accuracy, the combined self-consistent procedures, in which small fragments are described by the most reliable and suitable DFT approaches (e.g., for d/f elements) and their environment by more appropriate (e.g., economical) ones, are quite attractive alternatives to direct studying periodic systems or some of their extended fragments. However, combining WFT and DFT in one calculation is not trivial from a theoretical point of view since exchange and correlation effects are treated very differently in these theories. Therefore, some additional approximations are usually involved here as a local embedding potential model within a frozen-density embedding scheme (used, e.g., for the ground state WFT-in-DFT and DFT-in-DFT models) [60] or some other simplifications for the considered fragment [36]. In their turn, accurate WFT-in-DFT approaches can be rather consuming computationally for the fragments containing d/f elements of sufficiently large size when the local embedding potential model is used. For completeness, we also mention here about numerous semiempirical hybrid methods of molecular

modeling (e.g., see Ref. [63] and references therein) which are popular to study physical-chemical properties of complicated but specific actinide-containing structures, for which pure wave-function and/or DFT based methods are too consuming or cannot provide reliable results. In this regard, the semilocal (radially-local) pseudopotential techniques have proved to be quite a reliable toolkit to combine WFT-based frozen core approximation with DFT treatment of electronic structures in the valence region of chemical compounds when providing a very high accuracy of the calculations [40]. It is well known that semilocal pseudopotentials developed and well working in WFT studies manage also well in DFT calculations of small molecules. (Though, as discussed above, they are seriously modified to improve the computational efficiency of the plane-wave DFT studies with reducing the energy cutoff value, but these modifications are not actual for DFT studies with the localized basis sets.) This “practical” observation has theoretical justification since most accurate norm-conserving semilocal PPs, in fact, are localized in the atomic core region with $r < R_c$ except the Coulomb potential from the nucleus and core shells. As the original Coulomb potential from the nucleus and core of a given atom, these PPs are “hard” enough when acting on the *valence orbitals* in the *core region* (see Refs. [13,17] and references therein).

Finally, not only the original valence and low-lying virtual (W) atomic orbitals but corresponding “equivalent” pseudo-orbitals in the atomic core region ($r < R_c$) for a hard-core PP are practically proportional to each other for every angular electronic momentum l term in the scalar-relativistic approximation (and for every l, j term in the fully relativistic case, where j is total electronic momentum). In turn, the partial expansion coefficients for both the original valence orbitals and pseudo-orbitals are very close [13,17,64], whereas the radial dependence of the original W orbitals and pseudo-orbitals in the atomic core region ($r < R_c$) is, certainly, different when the pseudo-orbitals are smoothed. It means that for effective Hamiltonians with the hard-core semilocal PPs, the W part of the one-electron density matrix in the core region, $\rho^W(r, r')$ with $r < R_c$ and $r' < R_c$, can be rewritten in the one-center expansion form as that reduced on the radial quantum numbers (the AiC density matrix is introduced in Ref. [17] and the advanced AiC version for accurate description of effective states of d/f elements, with the pilot application in Ref. [22], is in progress now). Thus, it is sufficient to know only the AiC density matrix to calculate with good accuracy all the popular properties described by the operators localized in the atomic cores (see also the above discussion about the AiC properties). In turn, the AiC density matrix can be considered as an “intermediate construction” between the conventional WFT density matrix and electronic density used in DFT.

Note that the W orbitals of an atom in a given electronic state used in DFT (Kohn-Sham orbitals) are largely proportional to the W orbitals in WFT approaches in the atomic core region $r < R_c$ [17,18,22], so the effect of action of the hard-core semilocal PP term [the last term in Eq. (1)] both in WFT and DFT approaches is close as well (this thesis will be discussed in more detail in our further research). Moreover, the semilocal PP term is a relatively small correction to the local Coulomb term [the first two terms in Eq. (1)] that acts equivalently in WFT and DFT. Besides,

the relaxation properties (response) of the original atomic WF induced by external perturbations can be well reproduced by the atomic pseudo-wave function when the norm-conserving or shape-consistent PP is used [13], that is known also as the PP transferability [65]. Thus, the PPs can be considered as prospective “interfaces” between the wave-function based theories and DFT when providing minimal computational cost in simulation of a given fragment of a material explicitly with the embedding theories based on the semilocal PPs.

Furthermore, relativistic spin-dependent effects including Breit ones [66,67], quantum electrodynamics (QED) [68,69], and correlation effects [70,71] can be taken into account with high accuracy within the PP approximation and only in those regions (core or valence) in which they are important. In particular, the core-electron states can be frozen as atomic spinors, whereas the valence ones may be treated as spin orbitals (with the spin-orbit corrections often taken on the last computational stage only) [13]. Thus, the resource-consuming periodic calculations can be performed in the scalar-relativistic approximation, and the spin-orbit corrections can be then evaluated in the embedded cluster study. Even large-core PPs can well reproduce the original small relaxation of atomic electronic structures caused by small external perturbations if they are generated as “transferable” [65] and for appropriate *effective states* of the atom in a compound [17] (see also the next section). Therefore, such large-core PPs can be used to describe environmental atoms if their electronic structure is only slightly relaxed due to perturbations in the main cluster region. Taking into account that advanced small-core PP versions can also provide benchmark computational accuracy (as compared to all-electron four-component approximations due to better flexibility with the basis set choice when combining the effective spin-dependent Hamiltonians and scalar-relativistic ones) even for diatomic molecules containing heavy *d/f* elements (see Ref. [40] and references therein), the PP method can be considered as a universal and very flexible toolkit for studying the electronic structure of point defects with *d/f* elements.

In the paper, a method, *compound-tunable embedding potential* (CTEP), based on the PP theory is proposed to describe local properties and processes in minerals, particularly if the minerals contain point defects with *d/f* elements. The power of the method is demonstrated here on the calcium niobate crystal, CaNb_2O_6 , with point Ta and U defects, as a model representative of a large family of tantalum-niobate minerals. Application of CTEP to xenotime—yttrium orthophosphate mineral, YPO_4 , having both ionic and covalent bonds—is discussed in Ref. [15], where the thorium- and uranium-containing point defects are also studied. The other application of CTEP, to the structures containing periodically arranged lanthanide atoms with open *4f* shell, is considered in Ref. [72] in the examples of the YbF_3 and YbCl_3 crystals compared to the YbF_2 and YbCl_2 ones.

Calcium niobate crystal as the base of the fersmite mineral is of interest in several aspects. First, it was recently found in Refs. [73,74] that it can be successfully used as a direct indicator mineral for deposit targeting.

Second, fersmite has euxenite structure type (AB_2O_6), and there are reasons to believe that the hardened forms of high-level waste (HLW) based on minerals of the euxenite

group may have a higher chemical resistance compared to the pyrochlore-based forms of HLW storage, which attracted the most attention during recent decades as optimal immobilization matrices for HLW. It is shown in Ref. [75] that uranium(IV) is resistant to the effects of natural waters and practically does not participate in the processes of isotope fractionation. The leaching of radiogenic uranium occurs only after its transition to the pentavalent and hexavalent states. Thus, it can be expected that euxenite-based ceramic matrices, including tri- and tetravalent actinides, will be more resistant to the effects of natural fluids and, consequently, they can provide a more suitable approach to the long-term immobilization of actinides than matrices based on minerals of pyrochlore supergroup, in particular, betafite (see Ref. [76] and references therein).

Third, high optical and structural quality single calcium niobate crystal, grown by laser-heated pedestal growth technique directly from starting reagents [77], is of interest as a strong source of coherent light. It was noted fifty years ago [78] that this crystal can be used both as a laser and a laser host material and can be also useful in holography. The RE^{+3} -doped crystals (where RE stands for rare earth elements including Nd, La, etc.) with only a few percent RE cations as impurities attract much attention due to their unique and useful optical properties, and CaNb_2O_6 is one of the promising candidates here as a host crystal [33]. Studies of CaNb_2O_6 with RE impurities are assumed in the future.

At last, the leading component of fersmite, CaNb_2O_6 , has an orthorhombic unit cell and relatively simple structure compared to other minerals of the euxenite group and, therefore, it is chosen for our pilot CTEP study of the euxenite family of minerals. Substitution of niobium by tantalum (having high molar weight in fersmite) and calcium by uranium is considered in the paper.

II. CTEP METHOD

In the framework of the CTEP version of the embedding potential theory, the following procedure for calculating the electronic structure of a crystal fragment which can include a point defect is implemented:

(1) High-level periodic DFT calculation of a crystal without point defects.

(2) Cutting a fragment out of a crystal with a central metal atom/ion (which can be further replaced by a vacancy, impurity atom, etc.) and its nearest anionic environment. Thus, the first coordination sphere consists of a small number of atoms that is usually not more than 12 (as in the case of dense packing). This structure will be referred to further as the “main cluster.”

(3) For the main cluster, one can first choose a *nearest cationic environment*, NCE, from the lattice atoms (second coordination sphere, etc.) and then, a *nearest anionic environment*, NAE, including a set of all anions which are nearest to the NCE atoms except those of the main cluster. The main cluster together with the nearest environment, i.e., main cluster + NCE + NAE (or main cluster + CTEP), will be referred to as the *extended cluster*, or just a cluster.

The above procedure yields a cluster of a minimal possible size. However, such a model is not necessarily sufficient for

a particular study. In this case, one can select a larger set of atoms as the main cluster, provided that the overall pattern scheme (main cluster + NCE + NAE) is conserved, i.e., the outermost layer of the main cluster consists of anions only. This structure can be described as a “multicenter cluster,” which is constructed by selecting a combination of several cations with their first coordination spheres.

The required size of the cluster depends on which properties and processes are studied. It will be shown in the present paper that a cluster of minimal size can reproduce the geometry and electronic structure of a fragment of an original structure with a pretty good accuracy, but large (or spatially extended) perturbations, such as a charged point defect, require a considerably larger embedded cluster. The final criterion of an “ideal” cluster size is that its further increase does not influence noticeably on the geometry and electronic structure in the area of interest.

The NCE is described by means of PPs generated for cations $A_n^{X_n+}$, where “+” stands for a cationic state of atom A_n corresponding to the oxidation state (number) $+X_n$ (X_n runs over the natural numbers), such that all the electrons of the cations are treated within the PPs as core ones and below designated as 0ve-PPs/ $A_n^{X_n+}$ or just 0ve-PPs for simplicity. Thoroughly, the 0ve-PP/ $A_n^{X_n+}$ generated for a given AiC effective state (to take account of the specific core relaxation of A_n in a given chemical compound) is written as

$$\mathbf{U}_n^{\text{0ve,AiC}} = -X_n/r + V_L^n(r) + \sum_l^{l_{\max}} [V_l^n(r) - V_L^n(r)] \sum_{m=-l}^l |l, m\rangle \langle l, m|, \quad (1)$$

where standard expression for the spin-averaged semilocal (radially-local) PP operator is used (e.g., see Ref. [13] and references therein; here l and m mean angular momentum and its projection for one-electron states; $L > l_{\max}$, where l_{\max} is highest angular momentum for electrons in the atomic core). Emphasize that the 0ve-PPs can be considered as the “valence-electron-free” pseudopotentials for the $\{A_n^{X_n+}\}$ cations, assuming that we do not attach more electrons to the main cluster additionally to those already involved there in accordance with the oxidation numbers of the atoms constituting the main cluster in a given compound. In practice, the known schemes of population analysis on atom A_n will not give exact zeros for occupancies of its valence orbitals even on alkali metals and the degree of covalence for the ionic bonding should be taken into account at the 0ve-PP generation stage for NCE atoms in a compound to take account of the core relaxation.

Each NCE atom is described by the semilocal PP and fractional point effective charge. “Tuning” the 0ve-PPs for environmental cations is carried out self-consistently in the periodic DFT calculations of pure crystal to minimize displacement forces on atoms A_n and others in the unit cell at the optimized DFT geometry of the crystal obtained at step (1). The pseudopotentials $\mathbf{U}_n^{\text{0ve,AiC}}$ are constructed by us basically following the scheme for the “self-consistent” PP version proposed in Refs. [13,79] to fit the AiC effective state of the $A_n^{X_n+}$ cations in the crystal (details of the CTEP generation procedure will be described elsewhere and note only that it

is based on the “shape-consistent” PP generation scheme that provide its transferability [65]).

The expression for the CTEP used in the given research is as

$$\mathbf{U}_{\text{CTEP}}(\vec{r}) = \sum_{n \in \text{NCE}} \left(\mathbf{U}_n^{\text{0ve,AiC}}(\vec{r} - \vec{r}_n) + \frac{q_n}{|\vec{r} - \vec{r}_n|} \right) + \sum_{a \in \text{NAE}} \left(\frac{q_a}{|\vec{r} - \vec{r}_a|} \right), \quad (2)$$

where $\mathbf{U}_n^{\text{0ve,AiC}}$ are the PPs from Eq. (1) for the corresponding NCE cations $A_n^{X_n+}$ which are “tuned” to fit the effective states of atoms (cations) in a compound, AiC, according to the chosen main cluster and the crystal under consideration. Tuning the partial charges, negative $q_n = -|q_n|$ for cations and positive $q_a = +|q_a|$ for anions, reflect the “polarization” of those electronic shells which are treated implicitly for the NCE and NAE atoms in the compound and simulate in our current CTEP model the electric field of environment acting on the main cluster.

Emphasize that the nearest anionic environment is described here by only the Coulomb potentials from effective NAE charges (optimized together with NCE charges as described below), however, in general—when breaking the covalent bonds in crystals and modeling the complicated main clusters—the 0ve-PPs can also be used for the NAE atoms to simulate the crystal fragment with better accuracy [80,81]. For the same reason, the point partial charges can also be used on the sites of atoms from nearest environment in general.

Both the NAE and NCE charges located at the lattice sites are optimized when constructing the CTEP to reproduce the spatial structure of the main cluster as a fragment from the periodic study (at step 1) in the molecular-type calculation of the extended cluster with only point symmetry of the crystal fragment taken into account. Our current charge optimization criterion is a minimization of sum of squares of forces on atoms from the main cluster, with the constraint that the total charge of the extended cluster is fixed to zero (see subsection “Cluster calculations” below).

Note that relaxation of electronic structure in both main cluster and nearest environment regions is taken into account within CTEP when one considers processes and point defects localized on the main cluster though the coordinates of the environmental atoms are not changed. In turn, the structure and size of the main cluster and its nearest environment are not directly related to a unit cell. After the initial preparations (periodic structure calculations, etc.) are made and the generation of CTEP (in which the original crystal periodicity is taken into account) is performed, the further cluster studies with the CTEP are done with only the local symmetry taken into account, including those with the point defects. Moreover, the CTEP model can also be applied to a non-periodic system, for example, to calculate local properties of an atom in a large cluster by building a smaller cluster using CTEP (to be used, e.g., in the coupled-cluster study). To date, the approach allows one to study only localized properties in a limited class of compounds such as ionic-covalent crystals.

III. COMPUTATIONAL DETAILS

All calculations were performed using DFT method with the PBE0 functional. The solid-state and cluster calculations are performed with the CRYSTAL-17 package [82] and slightly modified SO-DFT code from the NWChem package [83].

The core pseudopotentials generated by our group [13] for the Ca and Nb atoms are used. The original basis sets, corresponding to these PPs (mentioned below as LQC—(8,8,7,2)/[6,6,4,2] for Nb and (5,5,4,1)/[5,5,4,1] for Ca) are cut and contracted for use in solid-state calculations (mentioned below as LQC-c—(5,5,5,2)/[3,3,2,2] for Nb and (4,3,3,1)/[3,3,3,1] for Ca).

The tuned 0ve-PPs with the basis sets combined from the valence orbitals of the original basis sets (LQC and LQC-c) and core exponents of the pseudo-orbital expansion generated in the present work are used for the Ca and Nb “pseudoatoms” treated as NCE. Further, we will refer to these basis sets as LQC-0, and LQC-0c, respectively.

The O_pob_TZVP_2012 basis set designated below as TZVP-a is used for oxygen atoms. For a comparison, calculation of the Nb-centered cluster, along with untruncated (LQC and LQC-0) versions of Ca and Nb basis sets, is carried out with an augmented version of TZVP basis for oxygen (introduced in Ref. [22]) and mentioned below as TZVP-b (12,7,2)/[6,4,2].

Since the main goal of the paper is to examine the quality of the cluster simulation of periodic structures within the CTEP approximation, all our cluster calculations (except evaluation of XES chemshifts) are performed without spin-orbit interaction for consistency with the periodic calculations using CRYSTAL package, in which only scalar-relativistic effects can be taken into account due to the software limitations. The influence of spin-orbit effects is discussed in more detail in Refs. [15,72].

IV. RESULTS AND DISCUSSIONS

A. Periodic calculations

The calcium niobate crystal belongs to the *Pcan* space group and consists of five nonequivalent atomic types: Ca, Nb, and three different O types. Both atomic positions and cell parameters are optimized with only crystal symmetry group fixed. The resulting structure is close to the experimental one with the average bond length error about 0.8%.

The most significant difference is for the specific Ca-O bond with an interatomic distance of 2.80 Å in the experimental structure vs 2.71 Å in the DFT optimized one. In both cases this interatomic distance is considerably larger than the sum of crystal radii [1.26 Å for Ca(VIII) and 1.24 Å for O(IV)], and it is *a priori* unclear whether the corresponding atoms should be considered as the neighbor ones or not, so, when constructing the calcium-centered clusters, we have considered both cases of the first coordination sphere: CaO₆ and CaO₈.

B. Cluster calculations

The clusters centered on both Ca and Nb cations are built together with CTEPs. As mentioned above, the number of the nearest neighbors of Ca atom in the calcium niobate, which should be included in the main cluster, is ambiguous, so, two

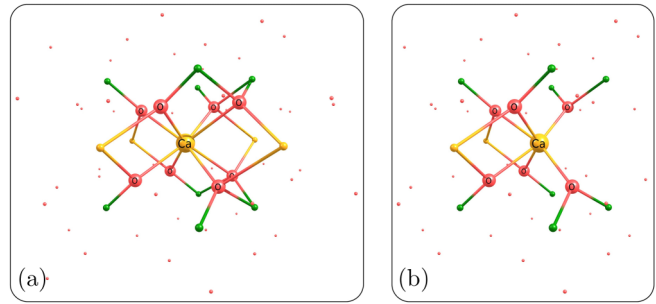


FIG. 1. Ca-centered clusters: (a) large $[\text{CaO}_8][\text{Ca}_4\text{Nb}_8][\text{O}_{44}]$ and (b) small $[\text{CaO}_6][\text{Ca}_2\text{Nb}_8][\text{O}_{38}]$. NCE atoms are shown as spheres of half radius without a caption (of the same color as for corresponding atoms of the main cluster and with the drawn bonds to the oxygen atoms) and NAE charges are shown as the dotlike semitransparent spheres.

main clusters with different CTEPs are built for the central calcium case: the small one, $[\text{CaO}_6][\text{Ca}_2\text{Nb}_8][\text{O}_{38}]$, and the large one, $[\text{CaO}_8][\text{Ca}_4\text{Nb}_8][\text{O}_{44}]$ (Fig. 1).

For the central Nb atom, only one cluster with CTEP, $[\text{NbO}_6][\text{Ca}_4\text{Nb}_6][\text{O}_{41}]$, is built. However, for a comparison, three stoichiometric clusters for the niobium surroundings (without CTEP) are built and considered. The first one is for a single minimal formula $[\text{CaNb}_2\text{O}_6]$, whereas the second and third ones are for four and eight minimal formulas, respectively (Fig. 2).

Despite that all the atoms for the stoichiometric clusters are treated on equal footing, for convenience of comparison we will refer to the central area (NbO₆ group) as the “main

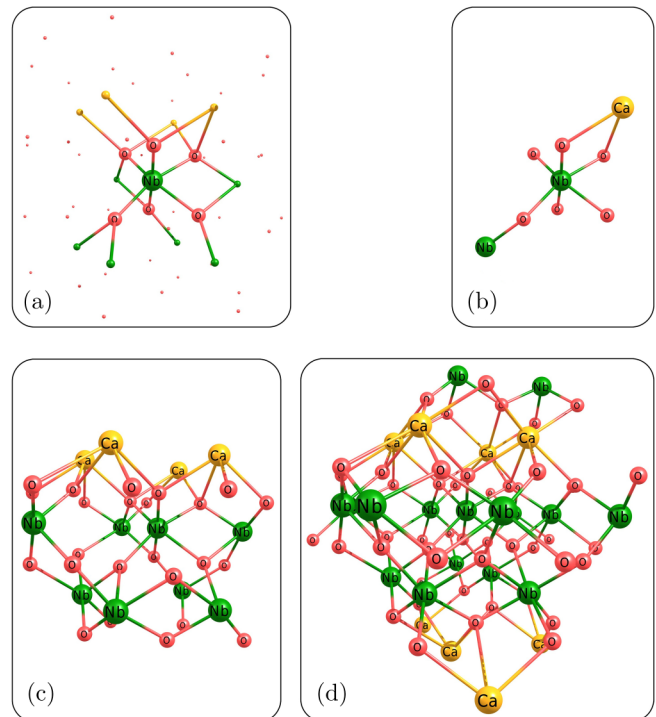


FIG. 2. Nb-centered clusters: (a) Cluster with CTEP, $[\text{NbO}_6][\text{Ca}_4\text{Nb}_6][\text{O}_{41}]$; (b)–(d) three stoichiometric clusters with one, four, and eight minimal formulas $[\text{CaNb}_2\text{O}_6]$, respectively.

TABLE I. Forces on the atoms of the main cluster and atomic displacements within the main cluster after its optimizations.

Structure	RMS force (a.u.)	RMS displacement (\AA)
Ca-CTEP-small	1.1×10^{-5}	1.5×10^{-4}
Ca-CTEP-large	2.6×10^{-5}	3.4×10^{-4}
Nb-CTEP	3.3×10^{-5}	2.6×10^{-4}
Nb-CTEP (<i>basis set 1</i>) ^a	3.2×10^{-3}	1.3×10^{-2}
Nb-CTEP (<i>basis set 2</i>) ^a	4.8×10^{-3}	1.5×10^{-2}
Nb-CTEP (<i>basis set 3</i>) ^a	4.9×10^{-3}	1.6×10^{-2}
Nb-stoichiometric (1 \times)	8.8×10^{-2}	2.0 ^b
Nb-stoichiometric (4 \times)	5.8×10^{-2}	8.8×10^{-1b}
Nb-stoichiometric (8 \times)	5.0×10^{-2}	1.9×10^{-1}

^aExtended basis sets, described in subsection ‘‘Cluster calculations.’’

^bStructure breaks after cluster optimization resulting in decrease of niobium coordination number.

cluster.’’ For each of the clusters with CTEP, the fractional charges on the cationic and anionic shells are optimized, and the resulting root mean square (RMS) forces on the main cluster are obtained. For a verification, the main cluster is re-optimized with fixed CTEP parameters and the resulting geometry is compared to the original one.

For the niobium-centered cluster with CTEP, optimization of geometry is additionally performed with three extended basis sets: (1) the same as for the periodic calculations except for the original uncut LQC basis on the niobium atom, (2) the LQC basis on the niobium atom with TZVP-b basis on oxygen atoms, and (3) the LQC basis on the niobium atom with TZVP-b basis on oxygen atoms and LQC-0 on the NCE atoms (see ‘‘Computational details’’ section for more information). Additionally, optimization of geometry was also performed for the stoichiometric clusters, with the central NbO₆ fragment being treated as the main cluster, and the remaining atoms are fixed as embedding ones.

For all the clusters the remaining forces after optimization of geometry are negligible. All the forces and displacements are listed in Table I.

For all the clusters with CTEP and original basis set, the forces and displacements are small enough allowing us to assume precise reproducibility of the geometry within the CTEP model. In the case of Nb cluster, expansion of basis set leads to an increase of both RMS forces and displacements by two orders of magnitude, however, the absolute numbers are still comparable to general errors of the DFT method. The agreement of cluster-optimized geometry with the experimental one stays on the same level as that for the crystal-optimized geometry.

For the stoichiometric clusters RMS forces are about three orders larger and only slowly decrease with the increase of a cluster size, so one can expect that it requires a much larger stoichiometric cluster to reproduce crystal structure at the same level as the CTEP method. Optimization of the stoichiometric clusters consisting of one and four formulas breaks the correct coordination number of central Nb, while the largest one (eight formulas) preserves the correct coordination number, but the displacements of corresponding atoms are significantly larger than those for the CTEP case.

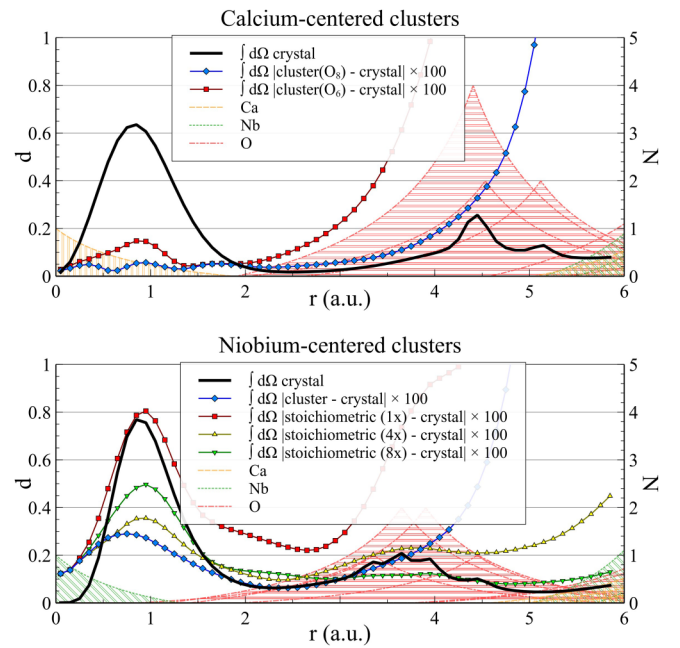


FIG. 3. The radial dependence of electronic density differences for the clusters under study. Thick black lines without markers represent total density. Colored solid lines correspond to the integral of absolute difference, $d(r)$, multiplied by a factor of 100. Filled dashed or dotted peaks at the bottom qualitatively represent the position of the neighbor atoms (color and line style denote atom type, width at the bottom is equal to crystal radius, and the peak height is proportional to the number of atoms (right vertical axis) at the same distance from the center).

Overall, we can state that the crystal fragment structure obtained in the periodic calculation within the chosen DFT approximation can be reproduced in the cluster calculation with CTEP without a notable decrease of the accuracy compared to the periodic DFT case, while the stoichiometric cluster approach yields much larger errors.

C. Electronic density comparison

To estimate the reproducibility of properties in the cluster model with CTEP, electronic density cube files were obtained for the periodic crystal study and for each cluster. The cube grid was chosen to be the same in all cases with the orthogonal unit vectors of about 0.056 a.u.

As a quantitative criterion we provide the difference between the cluster and crystal electronic densities, calculated by the following formula:

$$d(r) = \frac{1}{4\pi} \oint d\Omega |\rho_{\text{cluster}}(\vec{r}) - \rho_{\text{crystal}}(\vec{r})|.$$

In Fig. 3 this value is plotted for all clusters under study, except those with extended basis set. The bottom dashed peaks qualitatively represent the electronic density of atoms from the main cluster. The black curve is the total density, and all the difference curves are multiplied by factor 100, so that intersections between total and difference curves correspond to the 1% deviation.

For Ca-centered clusters the density in near surroundings of the central atom is reproduced with good accuracy. The larger cluster (with eight neighbors) both yields better agreement in the central area and preserves the tolerable error value in a larger radial range, which can be explained by the influence of the two oxygen atoms (at 5.1 a.u.), which are excluded from the smaller cluster.

The Nb-centered CTEP cluster yields a larger error in the vicinity of the central atom, while at larger R the difference is comparable to that of the eight-neighbor Ca-centered cluster. From comparison of the embedded Nb-centered cluster with the stoichiometric ones, it follows that the embedding model reproduces electronic density within $R < 3$ a.u. with notably better accuracy than any of the stoichiometric clusters, while being comparable by means of computational expenses to the smallest stoichiometric one. The considerable difference of electronic density in the central area compared to the solid-state one is almost the same for all Nb clusters, so it is likely to result not from the CTEP model inaccuracy but from computational features of the solid-state and cluster software (clarification of which in detail will be the subject of further research).

At $R \sim 4 \div 5$ a.u. the difference increases greatly for all the clusters with CTEPs, which reflects the matter of fact that outer core electrons of the cationic-layer atoms are included in the periodic calculations while being excluded from the cluster study using the 0ve-PPs, since the CTEP model is intended to describe only localized fragments of crystals. For both Ca- and Nb-centered clusters with CTEP the electronic density difference lies within 2% at the effective crystal radius (2.38 a.u. for Ca and 1.47 a.u. for Nb).

D. Chemical shifts of x-ray emission lines

Stabilization of computed internuclear distances with respect to a basis set enlargement is a good probe for the basis set saturation in the valence region of a compound when effective Hamiltonian and exchange-correlation functional are fixed. In turn, chemical shifts (chemshifts) of lines of x-ray emission (fluorescence) spectra, XES (see Refs. [84–86] and references therein), are sensitive to local variation of electronic densities in the atomic core regions [18] that cover probing the basis set completeness in theoretical study. Moreover, the XES chemshifts together with other AiC properties can provide a pretty informative array of data about the electronic structure near heavy d/f atoms in a solid. The energetic shifts of a characteristic transition between different core shells of an atom in a variety of compounds allow one to explore corresponding core regions [22] and study various AiC characteristics. In particular, the chemshifts of K_α lines of d/f elements are mainly sensitive to occupation numbers of appropriate d and f shells, whereas the chemshifts of K_β lines are already sensitive to distances to the ligands and their types. It is not less important that characteristic XES lines can be easily identified for any atom of interest and the XES chemshifts can be measured on the atoms having sufficient fraction in a material, thus providing data to characterize the effective state of *any* atom for all these compounds [17–19,22,87].

To estimate the XES chemical shift values on the Nb atom in the calcium niobate crystal with respect to a free Nb atom

TABLE II. X-ray chemical shifts on the Nb atom in clusters with CTEP (in meV).

Nb	Basis		Structure	$K_{\alpha 2}$	$K_{\alpha 1}$	$K_{\beta 2}$	$K_{\beta 1}$
	O	NCE					
LQC-c	TZVP-a	LQC-0c	crys ^a	345	364	227	246
LQC-c	TZVP-a	LQC-0c	opt ^b	345	364	226	246
LQC	TZVP-a	LQC-0c	crys ^a	344	362	221	235
LQC	TZVP-a	LQC-0c	opt ^b	341	359	213	227
LQC	TZVP-b	LQC-0c	crys ^a	348	366	235	247
LQC	TZVP-b	LQC-0c	opt ^b	346	364	236	248
LQC	TZVP-b	LQC-0	crys ^a	345	363	227	236
LQC	TZVP-b	LQC-0	opt ^b	343	361	225	235

^aOriginal structure (optimized in periodic calculation).

^bThe fragment structure, optimized in cluster calculation with the corresponding basis set.

we use the method described in Ref. [18]. At first, we compute the one-electron density matrix for only valence electrons taken into account in the cluster ρ_{clust}^V near the Nb nucleus and the valence density matrix ρ_{at}^V for the isolated Nb atom after the electronic structure calculations. To obtain these matrices we use the one-center restoration procedure described in Refs. [19,88]. The XES chemical shift can be represented as the difference between the average values of effective one-electron operator χ_{FI} , which describes the Coulomb interaction of valence electrons with the inner-core one in the final and initial states (after the x-ray induced Auger emission of the electron from the “final” state):

$$\langle \chi_{FI} \rangle = \sum \chi_{FI,rs} (\rho_{clust,rs}^V - \rho_{at,rs}^V),$$

$$\chi_{FI,rs} = (J_{I,rs} - K_{I,rs}) - (J_{F,rs} - K_{F,rs}). \quad (3)$$

In the above equation, indices r and s correspond to the valence states; $J_{I,rs}$ and $K_{I,rs}$ are the matrix elements of the angle-averaged direct (Coulomb) and exchange interaction of valence electrons with the electron in the initial state; $J_{F,rs}$ and $K_{F,rs}$ are those for the final state ones. By using this equation we obtain the XES chemical shifts values, which correspond to the vertical transition energies. This approximation is well justified for the transitions of the inner-core electron ($2p \rightarrow 1s$, $3p \rightarrow 1s$) in heavy atoms (see Ref. [18] for detailed discussion).

In Table II the chemshifts are presented for the Nb atom in the embedded cluster for four mentioned above basis sets and for the original structure “crys” (that is taken from periodic calculation) and re-optimized cluster structure after the CTEP construction (case “opt”).

The dispersion of the $K_{\beta 1,2}$ data is up to 10% with increasing the basis set size that is not negligible. Thus, the corrections on the incompleteness of the basis set in the crystal calculations are highly desirable. Such corrections can be rather easily evaluated for the main cluster of minimal size (with a central atom and first coordination sphere only) in contrast to the cases of large cluster or periodic structure studies.

In Table III the chemical shifts are presented for the Nb atom in the stoichiometric cluster with the periodic-optimized

TABLE III. X-ray chemical shifts on the Nb atom in stoichiometric clusters (in meV).

Cluster type ^a	Structure	$K_{\alpha 2}$	$K_{\alpha 1}$	$K_{\beta 2}$	$K_{\beta 1}$
Stoichiometric (1×)	crys	341	360	218	238
Stoichiometric (1×)	opt	234	249	89	102
Stoichiometric (4×)	crys	336	354	217	234
Stoichiometric (4×)	opt	171	171	-33	-29
Stoichiometric (8×)	crys	343	362	229	247
Stoichiometric (8×)	opt	353	373	267	285

^aThe basis set for all structures corresponds to the two upper rows in Table II—LQC-c for all Nb and Ca atoms and TZVP-a for O atoms.

(“original”) and cluster-optimized structures using DFT. The most important result of calculations of XES chemshifts with stoichiometric clusters is that the chemshifts for the cluster with even eight formulas cannot be considered as converged ones for K_{β} chemshifts to those of periodic structure (Table II) in contrast to those for the minimal cluster with CTEP despite that the XES chemshifts are considered on the central atom of all clusters used. One should also take into account that when increasing the cluster size, opportunities for its accurate treatment are dramatically diminishing because of problems both with the basis set completeness and correlation treatment quality on the wave-function level.

For an additional comparison of the cluster calculations with periodic ones, the Nb-centered cluster was calculated with the same parameters as in calculation with the CRYSTAL package (lesser basis set and all the pseudopotentials are used in spin-averaged approximation; the spin-orbit effects are taken into account in both cases only at final, one-center restoration stage [88] when calculating XES chemshifts). The XES chemshifts on Nb in calculations of the clusters relative to the crystal are presented in Table IV. As one can see, the difference between the periodic and cluster results does not exceed the overall errors of chemshifts estimate and, thus, cannot serve as a basis for inferences.

E. Three-center cluster

As was mentioned in the “CTEP METHOD” section, the minimal cluster is not the only possible one. Multicenter clusters allow one to take into account not only more structural and wave-function relaxations and perturbations around the crystal defect, but can also be used to study groups of closely located defects, such as compensating defects for a charged substitution, or clusters of the dope atoms, leading to fluorescence quenching [33].

TABLE IV. Difference of x-ray chemical shifts on the Nb atom between cluster calculations and the periodic one (in meV).

Structure	$K_{\alpha 2, \alpha 1}$	$K_{\beta 2, \beta 1}$
CTEP	3	9
Stoichiometric × 1	-1	0
Stoichiometric × 4	-7	-2
Stoichiometric × 8	1	9

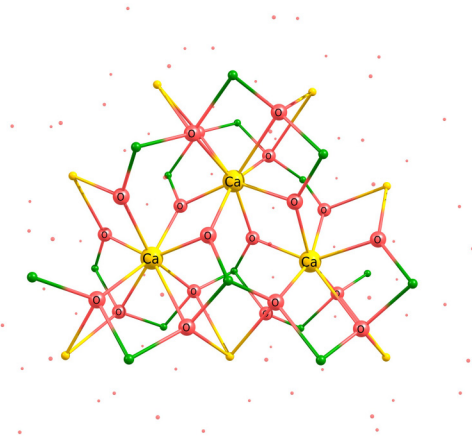


FIG. 4. 3-center cluster.

In the sections below we apply the CTEP for $\text{Ca} \rightarrow \text{U}$ substitution. As calcium and uranium have different oxidation numbers, these particular defects are charged ones. Two options are considered: a charged main cluster of minimal size (“1-center”) and a main cluster of larger size (in particular, “3-center”) which includes a compensating defect (a vacancy as a simplest case for U^{IV} and two vacancies for U^{VI}). The comparison of two approaches is used to estimate the required cluster size and general transferability of the CTEP model.

First, we need to construct the 3-center cluster for the ideal crystal. For this we took three nearby calcium atoms and all their neighbor oxygen atoms as the main cluster and repeated all the above mentioned steps to build the CTEP cluster. The 3-center cluster structure is shown in Fig. 4. The cluster has C_2 symmetry, with two calcium atoms being equivalent. These atoms will be denoted as the “side” atoms, and the remaining atom, lying on the symmetry axis, as the “central” one.

The 3-center cluster has a more complicated structure and, as a result, the CTEP model charge optimization is not as accurate as in the 1-center case. The RMS gradient was minimized only to 8.3×10^{-3} , while the RMS displacement after the subsequent optimization was found to be 5.9×10^{-2} , which is about two orders of magnitude more than for the 1-center clusters. The particular reasons for this are not yet studied in detail as this is a pilot application of CTEP model to multicenter clusters. However, the above RMS displacement is of the same order as the average difference between the experimental and DFT-optimized atomic positions in the periodic structure calculation, that is 6.5×10^{-2} for the same cluster. Thus, the RMS displacement errors are practically the same as the errors of periodic structure DFT calculations. The differences in electronic densities on both Ca types were found to be almost the same as for 1-center clusters, see Fig. 5. Thus, we consider this model as satisfactory to be used in simulation of point defects containing Ta and U atoms.

F. Point defects

1. Tantalum

As was mentioned above, the tantalum atoms are the most common substitutes of niobium ones in niobates, and the whole class of minerals is widely known as “tantalum

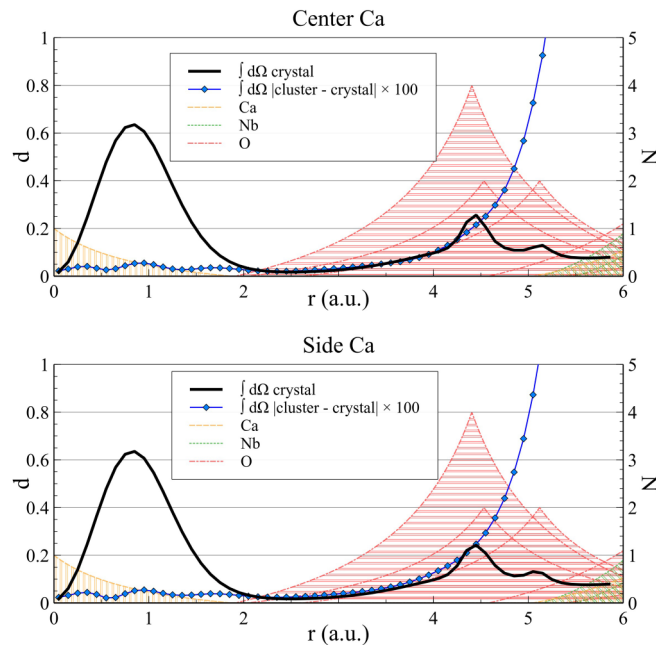


FIG. 5. Radial dependence of electronic density differences for both types of Ca atoms in the 3-center cluster.

niobates.” They are not just the elements from the same group in the periodic table, homologues, but their both chemical and structural properties are also very similar. In particular, the difference between their crystalline ionic radii [89] is of the same order as the experimental uncertainty in the internuclear distances. Taking into account that the molar fraction of Ta compared to Nb is about 15% in the fersmite mineral, it is natural to consider the Nb \rightarrow Ta substitution in the calcium niobate crystal to study its influence on the structural parameters of the mineral. The result of our calculations is the following: the RMS force at the calculated crystalline geometry of CaNb_2O_6 is 4.7×10^{-3} , while the RMS displacement after the embedded cluster optimization is only 1.0×10^{-2} . Such a small displacement is comparable with that going from the basis set incompleteness (due to necessity of its truncation in the crystalline study) in the DFT calculation of the calcium niobate and it does not considerably influence the crystal structure.

2. Uranium

Study of uranium defects is important due to the potential use of tantalum-niobate mineral as a matrix for radioactive waste. It was observed in Ref. [75], that the main oxidation states of uranium in niobates are IV and VI, and U substitutes the Ca atoms. The increase of the cluster size is also useful to study sustainability of the method for more complicated point defect cases as more structural relaxation is allowed.

In total, five types of clusters were considered and optimization of the main cluster geometry was performed for each one. Two clusters were built for a 1-center model: 1c- U^{IV} with total charge +2 and 1c- U^{VI} with total charge +4. Three clusters were considered for a 3-center model: 3c- $\text{U}^{\text{IV}}(\text{center})$ cluster with U in the central Ca site and a vacancy in the site of one of the side Ca atom, 3c- $\text{U}^{\text{IV}}(\text{side})$ cluster with U and

TABLE V. Distances to eight neighbor oxygen atoms, Å. “Ca” and “Ca(reopt)” are 3-center clusters with structures optimized in solid state and reoptimized with the CTEP model, correspondingly. Designations for the clusters with U defects are explained in the text.

n	Ca	Ca (reopt)	1c- U^{IV}	1c- U^{VI}	3c- $\text{U}^{\text{IV}}(\text{center})$	3c- $\text{U}^{\text{IV}}(\text{side})$	3c- U^{VI}
1	2.329	2.381	2.278	2.160	2.381	2.361	2.368
2	2.329	2.381	2.280	2.161	2.457	2.460	2.368
3	2.332	2.356	2.238	2.058	2.186	2.165	2.054
4	2.332	2.356	2.239	2.058	2.344	2.353	2.054
5	2.398	2.367	2.326	2.148	2.128	2.142	1.967
6	2.398	2.367	2.327	2.148	2.260	2.304	1.967
7	2.709	2.700	2.576	2.509	2.827	2.829	2.932
8	2.709	2.700	2.577	2.509	2.765	2.652	2.932

Ca as side atoms and a vacancy in the center, and 3c- U^{VI} with U in the center and two vacancies at the sides.

Table V lists the distances from the atom of interest (calcium for ideal crystal and uranium for the defect) to the nearest eight oxygen atoms. The ideal cluster structure undergoes serious changes in all the cases when the defect is introduced. There are two main factors which lead to a significant structure distortion in ionic crystals in general, including the change of the coordination numbers, in the case of impurities: (1) the change in the oxidation state and (2) the difference in the radii of corresponding ions. However, for the Ca \rightarrow U substitution in CaNb_2O_6 , the difference of Ca and U ionic radii [89] (1 Å in Ca^{2+} vs 1.1 Å in U^{4+} and 0.9 Å in U^{6+}) is not dramatic. Thus, the change in the oxidation state (+2 for Ca vs +4 and +6 for U) seems to us most important here.

The coordination number of Ca atoms in the ideal crystal is eight, with two of the neighbor oxygens located farther by about 0.35 Å than the other six. This qualitative neighbor arrangement remains almost the same, when U impurity is modeled by a charged single-center model. The only difference is in the decrease of all U-O bond lengths compared to Ca-O ones by 0.04–0.12 Å and 0.20–0.22 Å for U^{IV} and U^{VI} , correspondingly.

However, when the 3-center model is considered, the nearest six oxygen atoms become closer to the center, while the remaining two become farther or stay at about the same distance, so that the observed coordination number of U atoms is changed to six both for U^{IV} and U^{VI} . The difference in the results of 1-center and 3-center model calculations, combined with the fact that the latter allows one more structural relaxations, suggests that the U substitute atom in the niobate is likely to be six-coordinated. Even if the 3-center model is not precise enough (which can be investigated in a more detailed study), from the comparison of our results for the 1-center and 3-center clusters one can see that the minimal 1-center cluster model is not satisfactory to reproduce such a strong reorganization in the nearest environment of the impurity U atom.

The 3c- $\text{U}^{\text{IV}}(\text{center})$ and 3c- $\text{U}^{\text{IV}}(\text{side})$ models yield very similar neighbor arrangement for the U atom; this suggests that the multicenter CTEP model can reproduce the influence of environment on the fragment of the crystal on almost the same level for all centers included.

We do not consider here more subtle effects like different magnetic multiplets in the uranium atom since they cannot be easily separated from other interfering contributions in the given research. They will be first discussed in the theoretical studies of the xenotime embedded cluster of minimal size with the atomic actinide impurities in Ref. [80].

V. CONCLUSIONS

A new method to simulate a fragment of ionic-covalent crystals within the cluster model, *compound-tunable embedding potential*, CTEP, is applied to the calcium niobate crystal, CaNb_2O_6 , with impurity Ta and U atoms. The CTEP method is based on modeling the embedding potential by linear combination of short-range spherical Ove-PPs for the atoms composing the nearest environment of the main cluster, whereas the long-range CTEP part consists of only Coulomb potentials from environmental atoms. The short-range CTEP pseudopotentials for cations of the nearest environment are *tuned* for the given crystal (on the basis of self-consistent semilocal pseudopotential version [13]). The long-range CTEP part is determined by partial point charges centered on environmental atoms which are optimized as real numbers, positive for cations and negative for anions. The total (electronic and nuclear) charge of the extended cluster (main cluster and environment) is fixed to zero. The electronic structure relaxation of both the main cluster and boundary regions is taken into account within CTEP when one considers processes and point defects localized in the main cluster.

A pilot application of the CTEP method to the calcium niobate crystal is performed and a remarkable agreement of

the electronic density and optimized interatomic distances on the main cluster with those on the original crystal is attained. Characteristics of “atoms-in-compounds” [17], which are of primary interest for a compound of f and d elements (Nb in calcium niobate), are considered for chemical shifts of $K_{\alpha_{1,2}}$ and $K_{\beta_{1,2}}$ lines ($2p_{3/2,1/2} \rightarrow 1s_{1/2}$ and $3p_{3/2,1/2} \rightarrow 1s_{1/2}$, correspondingly) of x-ray emission (fluorescence) spectra from niobium.

This approach seems to us promising for studying properties of point defects in solids, vacancies, and impurities containing f and heavy d elements with relativistic effects and distortion of the crystal symmetry taken into account. Application of the approach to study adsorption of super-heavy elements on surfaces, effects of ionizing x-ray radiation, localized vibrations and rotations, magnetic structure of impurities of d/f elements in materials, new physics on ferroelectrics, etc., is in progress.

ACKNOWLEDGMENTS

The work on the GRECP generation for the light elements was supported by the personal scientific fellowship of N.S. Mosyagin of the governor of the Leningrad district. All the other studies were supported by the Russian Science Foundation (Grant No. 20-13-00225). We are grateful to R.V. Bogdanov, A.V. Zaitsevskii, S.G. Semenov, and I.V. Abarenkov for many fruitful discussions. Calculations in the paper were carried out using resources of the collective usage center “Modeling and predicting properties of materials” at NRC Kurchatov Institute - PNPI.

-
- [1] M. Chergui, *Struct. Dyn.* **3**, 031001 (2016).
 [2] S. Ghimire and D. A. Reis, *Nat. Phys.* **15**, 10 (2019).
 [3] G. Kresse and J. Furthmüller, *Phys. Rev. B* **54**, 11169 (1996).
 [4] S. J. Clark, M. D. Segall, C. J. Pickard, P. J. Hasnip, M. J. Probert, K. Refson, and M. C. Payne, *Z. Kristallogr.* **220**, 567 (2005).
 [5] D. Vanderbilt, *Phys. Rev. B* **41**, 7892 (1990).
 [6] P. E. Blöchl, *Phys. Rev. B* **50**, 17953 (1994).
 [7] N. Troullier and J. L. Martins, *Phys. Rev. B* **43**, 1993 (1991).
 [8] D. R. Hamann, *Phys. Rev. B* **88**, 085117 (2013).
 [9] G. Kresse and D. Joubert, *Phys. Rev. B* **59**, 1758 (1999).
 [10] A. P. Bartók and J. R. Yates, *Phys. Rev. B* **99**, 235103 (2019).
 [11] A. Floris, I. Timrov, B. Himmetoglu, N. Marzari, S. de Gironcoli, and M. Cococcioni, *Phys. Rev. B* **101**, 064305 (2020).
 [12] K. Lejaeghere, G. Bihlmayer, T. Björkman, P. Blaha, S. Blügel, V. Blum, D. Caliste, I. E. Castelli, S. J. Clark, A. Dal Corso, S. de Gironcoli, T. Deutsch, J. K. Dewhurst, I. Di Marco, C. Draxl, M. Du lak, O. Eriksson, J. A. Flores-Livas, K. F. Garrity, L. Genovese, P. Giannozzi, M. Giantomassi, S. Goedecker, X. Gonze, O. Grånäs, E. K. U. Gross, A. Gulans, F. Gygi, D. R. Hamann, P. J. Hasnip, N. A. W. Holzwarth, D. Iuan, D. B. Jochym, F. Jollet, D. Jones, G. Kresse, K. Koepnik, E. Küçükbenli, Y. O. Kvashnin, I. L. M. Locht, S. Lubeck, M. Marsman, N. Marzari, U. Nitzsche, L. Nordström, T. Ozaki, L. Paulatto, C. J. Pickard, W. Poelmans, M. I. J. Probert, K. Refson, M. Richter, G.-M. Rignanese, S. Saha, M. Scheffler, M. Schlipf, K. Schwarz, S. Sharma, F. Tavazza, P. Thunström, A. Tkatchenko, M. Torrent, D. Vanderbilt, M. J. van Setten, V. Van Speybroeck, J. M. Wills, J. R. Yates, G.-X. Zhang, and S. Cottenier, *Science* **351**, aad3000 (2016).
 [13] A. V. Titov and N. S. Mosyagin, *Int. J. Quantum Chem.* **71**, 359 (1999).
 [14] G. Kresse, M. Marsman, and J. Furthmüller, “Ab-initio Vienna Simulation Package: VASP the Guide,” (2018), subsection 10.2.7 “ f -elements” (the PAW potentials).
 [15] Y. V. Lomachuk, D. A. Maltsev, N. S. Mosyagin, L. V. Skripnikov, R. V. Bogdanov, and A. V. Titov, *Phys. Chem. Chem. Phys.* **22**, 17922 (2020).
 [16] K. Adhikari, A. Chakrabarty, O. Bouhali, N. Mousseau, C. S. Becquart, and F. El-Mellouhi, *J. Comput. Sci.* **29**, 163 (2018).
 [17] A. V. Titov, Y. V. Lomachuk, and L. V. Skripnikov, *Phys. Rev. A* **90**, 052522 (2014).
 [18] Y. V. Lomachuk and A. V. Titov, *Phys. Rev. A* **88**, 062511 (2013).
 [19] L. V. Skripnikov and A. V. Titov, *Phys. Rev. A* **91**, 042504 (2015).
 [20] A. V. Zaitsevskii, L. V. Skripnikov, and A. V. Titov, *Mendeleev Commun.* **26**, 307 (2016).

- [21] A. Oleynichenko, A. Zaitsevskii, S. Romanov, L. V. Skripnikov, and A. V. Titov, *Chem. Phys. Lett.* **695**, 63 (2018).
- [22] Y. V. Lomachuk, Y. A. Demidov, L. V. Skripnikov, A. V. Zaitsevskii, S. G. Semenov, N. S. Mosyagin, and A. V. Titov, *Optics and Spectroscopy* **124**, 472 (2018).
- [23] N. S. Mosyagin, *Nonlinear Phenom. Complex Syst.* **20**, 111 (2017).
- [24] N. S. Mosyagin, A. V. Zaitsevskii, L. V. Skripnikov, and A. V. Titov, *Int. J. Quantum Chem.* **116**, 301 (2016).
- [25] L. O. Jones, M. A. Mosquera, G. C. Schatz, and M. A. Ratner, *J. Am. Chem. Soc.* **142**, 3281 (2020).
- [26] I. V. Abarenkov and M. A. Boyko, *Int. J. Quantum Chem.* **116**, 211236 (2016).
- [27] D. I. Khomskii, *Transition Metal Compounds* (Cambridge University Press, Cambridge, 2014), p. 485.
- [28] P. Martin-Ramos and M. Ramos-Silva (Eds.), *Lanthanide-Based Multifunctional Materials*, Micro and Nano Technologies (Elsevier Science, Amsterdam, 2018).
- [29] A. Comotti, S. Bracco, and P. Sozzani, *Acc. Chem. Res.* **49**, 1701 (2016).
- [30] S. V. Dmitriev, E. A. Korznikova, Y. A. Baimova, and M. G. Velarde, *Phys. Usp.* **59**, 446 (2016).
- [31] A. Wickenbrock, H. Zheng, L. Bougas, N. Leefer, S. Afach, A. Jarmola, V. M. Acosta, and D. Budker, *Appl. Phys. Lett.* **109**, 053505 (2016).
- [32] E. Kannatey-Asibu, Jr., *Principles of Laser Materials Processing* (John Wiley & Sons, Ltd, Hoboken, NJ, 2009).
- [33] X. Gong, H. Zhu, Y. Chen, J. Huang, Y. Lin, Z. Luo, and Y. Huang, *Cryst. Growth Des.* **19**, 6963 (2019).
- [34] S. K. Lamoreaux, *Phys. Rev. A* **66**, 022109 (2002).
- [35] I. B. Khriplovich and S. K. Lamoreaux, *CP Violation without Strangeness* (Springer, London, 2011).
- [36] L. V. Skripnikov and A. V. Titov, *J. Chem. Phys.* **145**, 054115 (2016).
- [37] L. V. Skripnikov, N. S. Mosyagin, A. V. Titov, and V. V. Flambaum, *Phys. Chem. Chem. Phys.* **22**, 18374 (2020).
- [38] A. Zaitsevskii and A. V. Titov, *Int. J. Quantum Chem.* **113**, 1772 (2013).
- [39] C. Van Wüllen, *J. Comput. Chem.* **23**, 779 (2002).
- [40] L. V. Skripnikov and A. V. Titov, *J. Chem. Phys.* **142**, 024301 (2015).
- [41] L. F. Pašteka, E. Eliav, A. Borschevsky, U. Kaldor, and P. Schwerdtfeger, *Phys. Rev. Lett.* **118**, 023002 (2017).
- [42] L. Gyevi-Nagy, M. Kallay, and P. R. Nagy, *J. Chem. Theory Comput.* **16**, 366 (2020).
- [43] A. Oleynichenko, A. Zaitsevskii, L. Skripnikov, and E. Eliav, *Symmetry* **12**, 1101 (2020).
- [44] A. V. Oleynichenko, A. Zaitsevskii, and E. Eliav, in *Supercomputing*, Communications in Computer and Information Science, edited by V. Voevodin and S. Sobolev (Springer International Publishing, Cham, 2020), Vol. 1331, pp. 375–386.
- [45] G. Knizia and G. K.-L. Chan, *Phys. Rev. Lett.* **109**, 186404 (2012).
- [46] S. Wouters, C. A. Jimé nez Hoyos, and G. K. L. Chan, in *Fragmentation* (John Wiley & Sons, Ltd, Hoboken, New Jersey, 2017), Chap. 8, pp. 227–243.
- [47] D. Vollhardt, *Annalen der Physik* **524**, 1 (2012).
- [48] E. Z. Kuchinskii, I. A. Nekrasov, and M. V. Sadovskii, *Phys. Usp.* **55**, 325355 (2012).
- [49] I. Peschel, *Braz. J. Phys.* **42**, 267 (2012).
- [50] I. W. Bulik, G. E. Scuseria, and J. Dukelsky, *Phys. Rev. B* **89**, 035140 (2014).
- [51] B.-X. Zheng, J. S. Kretchmer, H. Shi, S. Zhang, and G. K.-L. Chan, *Phys. Rev. B* **95**, 045103 (2017).
- [52] S. Wouters, C. A. Jimé nez Hoyos, Q. Sun, and G. K.-L. Chan, *J. Chem. Theory Comput.* **12**, 2706 (2016).
- [53] H. Pham, V. Bernales, and L. Gagliardi, *J. Chem. Theory Comput.* **14**, 1960 (2018).
- [54] E. Fertitta and G. H. Booth, *Phys. Rev. B* **98**, 235132 (2018).
- [55] M. A. al Badri, E. Linscott, A. Georges, D. J. Cole, and C. Weber, *Commun. Phys.* **3**, 4 (2020).
- [56] C. Lupo, F. Jamet, W. H. T. Tse, I. Rungger, and C. Weber, *Nature Portfolio* (2021), doi: 10.21203/rs.3.rs-74027/v1.
- [57] H. Lee, E. Plekhanov, D. Blackburn, S. Acharya, and C. Weber, *Commun. Phys.* **2**, 49 (2019).
- [58] E. Plekhanov, P. Hasnip, V. Sacksteder, M. Probert, S. J. Clark, K. Refson, and C. Weber, *Phys. Rev. B* **98**, 075129 (2018).
- [59] J. Neugebauer, *J. Chem. Phys.* **131**, 084104 (2009).
- [60] S. Höfener, A. S. P. Gomes, and L. Visscher, *J. Chem. Phys.* **136**, 044104 (2012).
- [61] S. Höfener, A. S. P. Gomes, and L. Visscher, *J. Chem. Phys.* **139**, 104106 (2013).
- [62] P. K. Tamukong, Y. G. Khait, and M. R. Hoffmann, *J. Phys. Chem. A* **121**, 256 (2017).
- [63] A. L. Tchougréeff, *Hybrid Methods of Molecular Modeling* (Springer, Berlin or Heidelberg, 2008).
- [64] A. V. Titov, N. S. Mosyagin, A. N. Petrov, T. I. Isaev, and D. P. DeMille, in *Recent Advances in the Theory of Chemical and Physical Systems*, edited by J. P. Julien, J. Maruani, D. Mayou, S. Wilson, and G. Delgado-Barrio, Progress in Theoretical Chemistry and Physics Vol. 15 (Springer, Dordrecht, 2006), pp. 253–283.
- [65] S. Goedecker and K. Maschke, *Phys. Rev. A* **45**, 88 (1992).
- [66] A. N. Petrov, N. S. Mosyagin, A. V. Titov, and I. I. Tupitsyn, *J. Phys. B* **37**, 4621 (2004).
- [67] N. S. Mosyagin, A. N. Petrov, A. V. Titov, and I. I. Tupitsyn, in *Recent Advances in the Theory of Chemical and Physical Systems*, edited by J. P. Julien, J. Maruani, D. Mayou, S. Wilson, and G. Delgado-Barrio, Progress in Theoretical Chemistry and Physics Vol. 15 (Springer, Dordrecht, 2006), pp. 229–251.
- [68] V. V. Flambaum and J. S. M. Ginges, *Phys. Rev. A* **72**, 052115 (2005).
- [69] V. M. Shabaev, I. I. Tupitsyn, and V. A. Yerokhin, *Phys. Rev. A* **88**, 012513 (2013).
- [70] N. S. Mosyagin and A. V. Titov, *J. Chem. Phys.* **122**, 234106 (2005).
- [71] J. R. Trail and R. J. Needs, *J. Chem. Phys.* **139**, 014101 (2013).
- [72] V. M. Shakhova, D. A. Maltsev, Yu. V. Lomachuk, N. S. Mosyagin, L. V. Skripnikov, and A. V. Titov (unpublished).
- [73] D. Mackay, G. Simandl, W. Ma, M. Redfearn, and J. Gravel, *J. Geochem. Explor.* **165**, 159 (2016).
- [74] G. J. Simandl, J. A. Petrus, M. I. Leybourne, S. Paradis, and C. Akam, in *Geological Fieldwork 2018, British Columbia Ministry of Energy, Mines and Petroleum Resources*, British Columbia Geological Survey Paper 2019-01 (British Columbia Geological Survey, 2018), pp. 113–123.
- [75] M. H. Khanmiri and R. V. Bogdanov, *Radiochemistry* **60**, 79 (2018).

- [76] M. Hosseinpour Khanmiri, S. Y. Yanson, E. V. Fomin, A. V. Titov, A. V. Grebeniuk, Y. S. Polekhovsky, and R. V. Bogdanov, *Phys. Chem. Miner.* **45**, 549 (2018).
- [77] R. de Almeida Silva, A. de Camargo, C. Cusatis, L. Nunes, and J. Andreetta, *J. Cryst. Growth* **262**, 246 (2004).
- [78] J. P. Cummings and S. H. Simonsen, *Am. Mineral.* **55**, 90 (1970).
- [79] A. V. Titov and N. S. Mosyagin, *Struct. Chem.* **6**, 317 (1995).
- [80] Y. V. Lomachuk, D. A. Maltsev, N. S. Mosyagin, V. M. Shakhova, and A. V. Titov (unpublished).
- [81] D. A. Maltsev, Y. V. Lomachuk, N. S. Mosyagin, and A. V. Titov (unpublished).
- [82] R. Dovesi, A. Erba, R. Orlando, C. M. Zicovich-Wilson, B. Civalleri, L. Maschio, M. Rérat, S. Casassa, J. Baima, S. Salustro, and B. Kirtman, *Wiley Interdiscip. Rev.: Comput. Mol. Sci.* **8**, e1360 (2018).
- [83] M. Valiev, E. Bylaska, N. Govind, K. Kowalski, T. Straatsma, H. Van Dam, D. Wang, J. Nieplocha, E. Apra, T. Windus, and W. de Jong, *Comput. Phys. Commun.* **181**, 1477 (2010).
- [84] K. Siegbahn, in *Nishina Memorial Lectures*, Lecture Notes in Physics (Springer Japan, Osaka, 2008), Vol. 746, pp. 137–228.
- [85] O. I. Sumbaev, *Phys. Usp.* **21**, 141 (1978).
- [86] S. I. Bokarev and O. Kühn, *WIREs Computational Molecular Science* **10**, e1433 (2020).
- [87] V. M. Shakhova, Y. V. Lomachuk, Y. A. Demidov, L. V. Skripnikov, N. S. Mosyagin, A. V. Zaitsevskii, and A. V. Titov, *Radiation and Applications* **2**, 169 (2017).
- [88] A. V. Titov, N. S. Mosyagin, A. N. Petrov, and T. A. Isaev, *Int. J. Quantum Chem.* **104**, 223 (2005).
- [89] L. T. Bugaenko, S. M. Ryabykh, and A. L. Bugaenko, *Moscow Univ. Chem. Bull.* **63**, 303 (2008).